Autonomous sensing the insulin peptide by an olfactory G protein coupled receptor modulates glucose metabolism

Jie Cheng[#1], Zhao Yang[#2], Xiao-Yan Ge[#1], Ming-Xin Gao[1], Ran Meng[1], Jing-Yu Lin[1], Zhao-Mei Tian[1], Yun-Fei Xu[4], Fan Yang[1,2], Jin-Peng Sun*[2,3] and Xiao Yu*[1]

Affiliations:

[1]Key Laboratory Experimental Teratology of the Ministry of Education and Department of Physiology, School of Basic Medical Sciences, Shandong University, Jinan, Shandong 250012, China

[2]Department of Biochemistry and Molecular Biology, School of Basic Medical Sciences, Shandong University, Jinan, Shandong 250012, China

[3]Department of Physiology and Pathophysiology, School of Basic Medical Sciences, Peking University, Key Laboratory of Molecular Cardiovascular Science, Ministry of Education, Beijing 100191, China

[4]Department of General Surgery, Qilu Hospital of Shandong University, Jinan, Shandong 250012, China.

[#] These authors contributed equally to this work

* Corresponding author: Jin-Peng Sun (corresponding author)
E-mail: sunjinpeng@sdu.edu.cn
Xiao Yu (corresponding author)
E-mail: yuxiao@sdu.edu.cn

Abstract

Along with functionally intact insulin, diabetes-associated insulin peptides are secreted by β cells(*1-3*). By screening the expression and functional characterization of olfactory receptors in pancreatic islets, we identified Olfr109 as the receptor to detect insulin peptides. Engagement of one insulin peptide, insB:9-23, with Olfr109 diminished insulin secretion through Gi-cAMP signalling and promoted macrophage proliferation. Remarkably, Olfr109 deficiency alleviated intra-islet inflammatory responses and improved glucose homeostasis in *Akita*- and HFD-fed mice. We further determined the binding mode between the insB:9-23 and Olfr109. A pepducin-based Olfr109 antagonist improved glucose homeostasis in diabetic and obese mouse models. Collectively, we found that pancreatic β cells use Olfr109 to autonomously detect self-secreted insulin peptides and this detection arrests insulin secretion and crosstalk with macrophages to increase intra-islet inflammation.

Introduction

Animals detect and interpret odourant information through a family of G protein-coupled receptors (GPCRs) called olfactory receptors (ORs); ORs constitute one of the largest mammalian gene families, with approximately 370 genes in humans and 800 in mice(*4-6*). In addition to playing a dominant role in odour detection, several ORs have been identified in organs other than the nasal olfactory epithelium, where they carry out distinct physiological functions, such as mediating sperm chemotaxis, muscle generation, cancer cell growth inhibition, hair growth, hepatic steatosis and adipose tissue lipolysis(*6-9*). However, the gene expression profiles and functions of ORs in pancreatic islets, where the glucose-regulating hormones insulin and glucagon are secreted, remain largely unknown.

Pancreatic islets are the only cellular factories producing insulin, which accounts for approximately 10% of the total protein content in pancreatic β cells. Recent studies showed that not only intact insulin molecules but also insulin peptide fragments are stored in pancreatic β cell vesicles and released into the circulation in response to glucose stimulation(*2*). Several of these insulin peptide fragments, as well as denatured insulin, act as antigens to trigger islet autoimmunity, which is functionally associated with the incidence of both type 1 diabetes (T1D) and type 2 diabetes(*10, 11*). Notably, these insulin peptide fragments bind poorly to MHC molecules, with micromolar affinity, in contrast to the relatively low (nanomolar) circulating concentration of insulin peptide in plasma(*12, 13*). Whether pancreatic β cells have developed a mechanism for detecting these insulin fragments and initiating signalling cascades to modulate the metabolic state remains elusive. Linking these islet secretions with their potential high-affinity receptors (e.g., GPCRs) and examining their corresponding functions will be highly valuable for understanding mechanism regulating islet homeostasis and for developing novel anti-diabetic strategies.

In the present study, we identified six ORs with high expression levels in islets. One of these ORs, Olfr109, was expressed in pancreatic islets, as supported by the RNAscope *in situ* hybridization, mRNA levels of GFP-labeled selective pancreatic cell types, as well as specific radio-ligand binding. Olfr109 was the receptor for the endogenous pancreatic peptide insB:9-23 or denatured insulin, modulating insulin secretion from pancreatic islets through Gi-cAMP signalling and manipulating CCL-2 levels to communicate with islet-resident macrophages, which resulted in increased macrophage proliferation. Consistent with these observations, Olfr109 knockout mice fed a high-fat diet (HFD) or on the Akita diabetic mouse background showed improved glucose metabolism, increased insulin secretion and ameliorated inflammatory responses within islets. We characterized the ligand-receptor interaction mode of Olfr109 and further developed a pepducin-based antagonist of Olfr109, which exhibited significant therapeutic potential for diabetes and obesity in mouse models.

Results

Expression of ORs in pancreatic islets

ORs are encoded by more than 300 genes in humans and approximately 800 genes in mice. To comprehensively assess human-related ORs with high expression levels in mouse islets, we designed PCR primers specific for all 278 mouse ORs that share more than 80% sequence identity with their closest human homologue and screened the expression levels of the corresponding mRNAs (Fig. S1A and Auxiliary Supplementary Table 1). With a cut-off expression level of more than 1% of the corresponding expression level in nasal tissue, only six ORs were detected in isolated mouse pancreatic islets: Olfr31, Olfr109, Olfr110, Olfr1335, Olfr1420 and Olfr1502 (Fig. 1A-1B and Fig. S1B). We then examined the changes in the expression levels of these receptors under physiological stimulation with high glucose and in mouse models of diabetes or obesity, including streptozotocin (STZ)- or L-Arg-treated mice, Akita mice, nonobese diabetic (NOD) mice and HFD model mice. In response to high-glucose stimulation, the expression level of all six ORs increased significantly in both human and mouse islets (Fig. 1C-1D and Fig. S2A). Intriguingly, in contrast to the differential expression changes in Olfr31, Olfr110, Olfr1335 and Olfr1502 in the different pathogenic models, only Olfr109 exhibited increased expression in all models of diabetes or obesity (Fig. 1C-1E and Fig. S2A-S2D).

We next preliminarily investigated the functions of these six ORs by overexpressing them in MIN6 pancreatic β cells. Whereas overexpression of all 6 ORs was achieved in MIN 6 cells, only Olfr109 and Olfr110 could be detected on the plasma membrane (Fig. S2E-S2F). Specifically, overexpression of Olfr109 but not Olfr110 in MIN6 cells decreased insulin secretion in response to stimulation with high glucose or a combination of high glucose and GLP-1 (Fig. 1F). In addition, decreased expression of the pancreatic β cell proliferation markers mki67, ccnb1, and cdk4 and increased expression of the stress response genes prdx5, sxbp1 and grp78 were observed in cells overexpressing *Olfr109* but not in cells overexpressing Olfr110 (Fig. S2G-S2J). Moreover, the highest expression of *Olfr109* was found in pancreatic islets and spleen compared with all other examined tissues except nasal tissue (Fig. S1B). The specific changes in expression levels in pancreatic islets and the preliminary functional differences observed by overexpression of Olfr109 in pancreatic β cell lines prompted us to explore the potential functions of Olfr109 in depth.

Improved glucose homeostasis in *Olfr109*-deficient mice in a model of diabetes

We used the RNAscope *in situ* hybridization to investigate the expression of *Olfr109* in pancreatic islets and generated the *Olfr109*-deficient (*Olfr109*$^{-/-}$) mice by the CRISPR-Cas9 system to study the *Olfr109* function (Fig 1G, Fig. S3A-S3C). *Olfr109* mRNA was mainly distributed within insulin-expressing cells in the islets of WT mice, but not in those of

Olfr109$^{-/-}$) mice. This data was consistent with the significant higher mRNA detected in the *Ins2*-Cre:GFP$^{f/f}$ labeled pancreatic β cells than that of *gcg*-Cre:GFP$^{f/f}$ labeled α cells or sst-cre$^{+/-}$GFP$^{f/f}$ labeled δ cells (Fig. S3D).

To explore the role of *Olfr109* in metabolism, we investigated glucose and energy homeostasis in *Olfr109*$^{-/-}$ mice. The body weight, energy expenditure and respiratory quotient were similar between *Olfr109*$^{-/-}$ mice and wild-type mice (Fig. 1H-1J). We then crossed *Olfr109*$^{-/-}$ mice with *Akita* mice, a neonatal model of diabetes mimicking maturity-onset diabetes of the young (MODY) in humans (Fig. S3E)(*14*, *15*). Compared with wild-type mice, *Akita* mice have a significantly decreased weight, exhibit increased energy expenditure in the dark photoperiod and present reduced respiratory quotient values at 2- to 3-months of age. Importantly, knockout of *Olfr109* almost completely reversed all of these effects. Moreover, *Olfr109* deficiency markedly improved glucose tolerance and glucose-induced plasma insulin levels in ins2$^{WT/Akita}$*Olfr109*$^{-/-}$ mice compared with ins2$^{WT/Akita}$ mice at 8 weeks (Fig. 1K-1L). Adult Akita mice are used as a model of severe insulin-deficient diabetes, with a reduction in insulin content of approximately 80%-90%. Deficiency of *Olfr109* significantly compensated for the loss of insulin content in the *Akita* background (Fig. 1M). Consistent with this observation, islets derived from Ins2$^{WT/Akita}$*Olfr109*$^{-/-}$ mice showed stronger immunostaining for PDX1 and NKX6.1, two important identity markers of pancreatic β cells than islets derived from ins2$^{WT/Akita}$ mice (Fig. S3F-S3G, Auxiliary Supplementary Fig. 1). Notably, recent studies showed that myeloid lineage-derived CD11c^{+} macrophages are specifically expanded inside the islets of HFD-fed mice, which correlated with increased islet inflammation and contributed to impairment of pancreatic β cell functions. Similar to the finding in HFD-fed mice, the population of CD11c^{+} macrophages in the islets of *Akita* mice was markedly increased by approximately 3-fold compared with that in wild-type mice. Knockout of *Olfr109* significantly reduced this effect (Fig. 1N). These results indicated that *Olfr109* negatively regulated glucose homeostasis in this diabetic model and that deletion of *Olfr109* significantly enhanced the relief of diabetic symptoms.

Improved glucose homeostasis in *Olfr109*-deficient mice in a model of obesity

We then examined the role of *Olfr109* in obesity in an HFD-fed model. HFD feeding resulted in greater weight gain in *Olfr109*$^{-/-}$ mice than in wild-type mice after 13 weeks of age (Fig. 2A). Consistent with this result, HFD-induced *Olfr109*$^{-/-}$ mice showed increased energy expenditure compared with their HFD-induced wild-type littermates at 12 weeks old. The increased energy expenditure of HFD-fed *Olfr109*$^{-/-}$ mice may explain their lower weight gain (Fig. 2B). Moreover, HFD-induced *Olfr109*$^{-/-}$ mice exhibited increased respiratory quotient values (Fig. 2C), suggesting that glucose utilization was enhanced in mutant mice compared

with wild-type mice under HFD stress, potentially due to the decrease in insulin sensitivity under these conditions (Fig. 2C). Notably, no significant differences in locomotor activity or food intake were observed between *Olfr109*$^{-/-}$ mice and wild-type mice (Fig. S4A-S4C).

At 12 weeks, the white adipose tissue and liver weights were significantly lower in HFD-fed *Olfr109*$^{-/-}$ mice (Fig. S4D-S4E). A significant decrease in the epididymal adipocyte size in the HFD-fed *Olfr109*$^{-/-}$ mice was observed by H&E staining (Fig. S4F). In addition, both the number of F4/80-positive cells in epididymal tissue and the liver steatosis were reduced in *Olfr109*$^{-/-}$ mice compared to their wild-type littermates under HFD stress (Fig. S4G-4H). These decreases were consistent with the decreased insulin resistance of *Olfr109*$^{-/-}$ mice at 13 weeks under HFD stress (Fig. 2D). However, whereas HFD-fed *Olfr109*$^{-/-}$ mice exhibited improved glucose metabolism in the glucose tolerance test (GTT) at a time point as early as 6 weeks (Fig. 2E and Fig. S4I), the difference in insulin resistance between the mutant mice and the wild-type mice was not observed at this early time point (Fig. S4J). These observations indicated that the change in glucose tolerance occurs before the improvement in insulin resistance in HFD-fed *Olfr109*$^{-/-}$ mice. Moreover, whereas the level of plasma GLP-1 did not differ significantly (Fig. S4K), fasting glucose, insulin and leptin levels were lower in HFD-fed *Olfr109*$^{-/-}$ mice (Fig. S4L-S4N). Importantly, the plasma glucose level was decreased and the insulin level was significantly increased after refeeding, which may account for the improved glucose tolerance test results in the HFD-fed *Olfr109*$^{-/-}$ mice (Fig. 2F-2G).

The earlier onset of changes in glucose tolerance test than in the insulin tolerance test (ITT) in HFD-induced *Olfr109*$^{-/-}$ mice and the improvement in insulin secretion after refeeding indicated that Olfr109 deficiency may enhance glucose homeostasis in HFD-treated mice through regulation of pancreatic islet functions. Consistent with this hypothesis, high glucose-induced insulin secretion was markedly increased under both normal culture and HFD-induced conditions in pancreatic islets isolated from *Olfr109*$^{-/-}$ mice compared to those isolated from their wild-type littermates (Fig. 2H and Fig. S4O). Whereas the size distributions of α and δ cells in islets did not differ significantly between *Olfr109*$^{-/-}$ mice and their wild-type littermates under HFD stress (Fig. S5A-S5B), *Olfr109*$^{-/-}$ mice had more islets with a size between 50-100 μm than wild-type mice (Fig. S5C-S5D). Moreover, the expansion of intra-islet CD11c^{+} macrophages and level of co-immunostaining of glucagon with insulin were significantly reduced in islets derived from *Olfr109*$^{-/-}$ mice compared with islets derived from their HFD-fed wild-type littermates (Fig. 2I-2J and Auxiliary Supplementary Fig. 2A). These results indicated that Olfr109 promoted dedifferentiation of pancreatic β cells and obesity-associated islet metaflammation (*16*).

Identification of the insB:9-23 peptide and denatured insulin as *Olfr109* agonists

To gain a preliminary understanding of Olfr109-mediated signalling, we performed quantitative comparative transcriptome analysis in MIN6 cells with or without high-glucose stimulation by knocking down *Olfr109* expression in these cells and comparing them with control cells. Kyoto Encyclopedia of Genes and Genomes (KEGG) pathway analysis indicated that genes enriched in metabolic pathways, calcium signalling pathways and pathways regulating stem cell pluripotency showed significant changes depending on *Olfr109* expression (Fig. S6A-6C). In particular, components of the Gs/Gi-cAMP signalling network were also altered (Fig.3A-3B). Selective G protein subtypes are the main downstream transducers mediating OR functions(*17-19*). Consistent with this role, overexpression of Olfr109 caused notable inhibition of cAMP that was blocked by pertussis toxin (PTX), a Gi/Go inhibitor, indicating constitutive Gi coupling to Olfr109 (Fig. S6D).

Suspecting that an endogenous ligand is already present in islet of Langerhans cells, we next stimulated *Olfr109*-overexpressing HEK293 cells with pancreatic islet supernatant and examined its effects on Gs and Gi signaling. Importantly, *Olfr109*-overexpressing cells incubated with islet supernatant collected under high-glucose conditions but not with islet supernatant collected under low-glucose conditions exhibited significant inhibition of forskolin (FSK)-induced cAMP elevation in a concentration-dependent manner (Fig. 3C). In addition, incubation with supernatant collected under high-glucose conditions promoted recruitment of β-arrestin-1, another important regulator of GPCR signal transduction(*20-22*) , to YFP-tagged *Olfr109* (Fig. 3D and Fig. S6E). Moreover, supernatant from pancreatic islets derived from diabetic model Akita mice induced significantly higher Olfr109 activity than that derived from wild-type mice in both the cAMP assay and arrestin recruitment assay (Fig. 3C-3D). Collectively, these results indicated that an endogenous agonist of *Olfr109* eliciting the activity of both Gi and arrestin is present in pancreatic islet supernatants and that this specific agonist is present at a higher level in the Akita diabetic mouse model.

High glucose levels mobilize insulin-containing vesicles to the membrane and finally release them into the intercellular space in pancreatic islets. We therefore fractioned the secretory granules by differential centrifugation. Compared to the fraction obtained by centrifugation at 25000×g (the 25k fraction), the fraction obtained by centrifugation at 5000×g (the 5k fraction) showed an approximately 100-fold increase in potency and a 2-fold increase in Emax, suggesting enrichment of the *Olfr109* agonist in the 5k fraction (Fig. 3E-3F). Separation of the soluble 5k fraction with a 3 kD molecular weight cut-off filter indicated that the Olfr109 agonist has a relatively low molecular weight and could be a peptide-like substance (Fig. 3G-3H). We therefore performed mass spectrometry analysis to characterize the side-by-side peptidomes of the 5k fraction from pancreatic islets derived from both Akita and wild-type mice. A total of 40 peptides derived from 12 proteins were found to be enriched in the fraction from Akita mice by more than 2-fold compared with their

levels in the fraction from wild-type mice (Table S1, Auxiliary Supplementary Table 2).

We then synthesized the top 15 peptides and assessed their ability to activate *Olfr109*. Only the InsB-derived peptides, not the other identified peptides, showed significant cAMP inhibition and arrestin recruitment activity via *Olfr109* (Fig. 3I-3J, Fig. S6I-S6J, and Table S1). The most efficient InsB peptide, insB9-23, had a measured EC50 of 2.08±0.50 nM (Fig. 3I-3K and Table S2-S3). The ability of insB 9-23 to promote Gi coupling to *Olfr109* was further verified by a G protein dissociation assay (Fig. S6F). Activation of Olfr109 by insB 9-23 was determined to be specific because insB 9-23 showed no cross-activity with Olfr110 or other receptors with known peptide agonists (Fig. S6G-S6H). Moreover, saturation binding analysis of ^{125}I-insB 9-23 confirmed the specific interaction of the ligand with the membrane fractions of pancreatic islets of wild-type mice, in MIN6 pancreatic β cells and in HEK293 cells overexpressing *Olfr109* (*B*max, 11.01±0.57×10^3 cpm and *Kd*, 3.61±0.03 nM; *B*max, 2746.00±92.73 cpm and *Kd*, 3.24±0.28 nM; and *B*max, 22.52±0.42×10^3 cpm and *Kd*, 4.11±0.07 nM, respectively) but not in islets derived from *Olfr109*$^{-/-}$ mice or in control HEK293 cells (Fig. 3L, Fig. S6M-O). Further whole-cell competitive binding assays of HEK293 cells overexpressing *Olfr109* revealed two binding affinities with a K_{Hi} of 2.73±0.07 nM and a K_{lo} of 109.95±0.15 nM (Fig. 3M). The observed K_{Hi} was similar to the EC50 of insB 9-23-induced Gi activity via *Olfr109*. The specific binding of the OLFR109 by the ^{125}I-insB 9-23 enabled us to determine the protein levels of OLFR109 in different tissues, which was correlated well with the mRNA levels of *Olfr109* (R^2=0.90), further confirming the specific endogenous expression of OLFR109 in pancreatic islets (Fig. 3N, Fig. S6M).

Previous studies have revealed that insB:9–23, which overlaps with the exposed region of denatured insulin, is a dominant epitope recognized by autoreactive T cells in both NOD mice and patients with type 1 diabetes(*2*, *23-25*). We therefore measured the response of *Olfr109* to denatured insulin. The EC50 of denatured insulin was 32.4±1.7 nM in the cAMP assay, and denatured insulin had a higher arrestin bias than insB 9-23 (Fig. S6K-S6L and Table S2). Considering that the insB 9-23 concentration ranges from 10 pM to 2 nM under physiological or pathological conditions (*2*) and that denatured insulin is more enriched in Akita mice than in wild-type mice and activates Olfr109 more potently, our collective results demonstrated that both insB 9-23 and denatured insulin are potential endogenous agonists of *Olfr109* in different physiological and pathological processes.

Modulation of pancreatic islet function and homeostasis via engagement of insB:9-23 with Olfr109

insB:9-23 is a dominant epitope recognized by T cells in diabetic patients and mouse models.

Free insB 9-23 was found not only to be presented to immune cells but also to circulate to peripheral organs through the circulatory system(*2*). However, the role of insB 9-23 in signalling has not been characterized. We next investigated the mechanism by which engagement of insB:9-23 with Olfr109 regulates pancreatic islet functions and glucose homeostasis. In primary pancreatic islets, administration of glucose and GLP-1 markedly increased insulin secretion; however, this effect was significantly dampened by incubation with insB:9-23 (Fig. 4A). Whereas overexpression of Olfr109 in primary pancreatic islets greatly reduced the insulin secretion elicited by combination treatment with GLP-1 and high glucose concentrations (Fig. S7A-S7C, Auxiliary Supplementary Fig. 2B), insulin secretion stimulated by high glucose concentrations either alone or in combination with GLP-1 was greatly increased in *Olfr109*$^{-/-}$ islets (Fig. 4A). Importantly, the inhibitory effect of insB:9-23 on insulin secretion was completely abolished in *Olfr109*$^{-/-}$ islets (Fig. 4A). GLP-1 promotes insulin secretion by mobilizing intracellular cAMP in pancreatic β cells(*26*). Consistent with this observation, we found that insB:9-23 strongly reduced the intracellular cAMP level in islets in response to GLP-1 stimulation and that this reduction was abolished in *Olfr109*$^{-/-}$ islets (Fig. 4B and Fig. S7D).

Moreover, whereas injection of insB:9-23 every other day for seven consecutive days resulted in glucose intolerance, Olfr109 deficiency reversed this effect (Fig. 4C). We therefore performed transcriptome analysis on islets from both *Olfr109*$^{-/-}$ mice and wild-type mice after insB:9-23 treatment. Importantly, the genes involved in chemokine signalling pathways, including Ccl2 and Ccl25, were highly upregulated in islets treated with insB:9-23 compared with islets from vehicle-treated mice (Fig. 4D). Both chemokines are reported to be involved in macrophage proliferation and infiltration(*27, 28*). In particular, Ccl2 has been linked to macrophage proliferation and infiltration in pancreatic islets and plays important roles in islet inflammation and pancreatic β cell dysfunction(*29, 30*). Notably, the insB:9-23-stimulated increases in chemokine levels were significantly reduced in *Olfr109*$^{-/-}$ mice (Fig. 4E). Consistent with the changes in these chemokine levels, insB:9-23 treatment increased the accumulation of macrophages in pancreatic islets by approximately 3-4-fold, and this increase was significantly reduced in *Olfr109*$^{-/-}$ mice (Fig. 4F and Fig. S7G).

We noted that Olfr109 was expressed mainly in pancreatic β cells but not in islet-resident macrophages (Fig. 4G). Islets cultured in vitro with supernatants collected from islets of HFD-induced wild-type mice showed markedly increased macrophage proliferation compared with islets cultured with supernatants collected from the corresponding *Olfr109*$^{-/-}$ mice (Fig. 4G-4H), indicating that Olfr109-mediated cellular events in islet β cells generate signals to induce macrophage proliferation, which contributed to the increased inflammation in HFD-induced model mice. Notably, not only was the Ccl2 mRNA level increased in insB:9-23-treated pancreatic islets, the Ccl2 protein level was augmented in islet supernatant after insB:9-23 treatment, and this increase was diminished by Olfr109 deficiency (Fig. 4I). We therefore hypothesized that Olfr109-mediated insB:9-23 activity caused increased

295 production of Ccl2, which is the main driving force for the proliferation of pancreatic
296 islet-resident macrophages through its interaction with the chemokine receptor CCR2.
297 Consistent with this hypothesis, administration of INCB3344, a CCR2 antagonist,
298 significantly blocked the promotive effect of insB:9-23 on macrophage proliferation, as
299 indicated by the reduction of both numbers of CD11c-positive intra-islet macrophages and
300 mRNA level of proliferative marker Ki67 (Fig. 4J-K and Fig. S7H). Therefore, engagement of
301 insB:9-23 upregulated the Ccl2-CCR2 chemokine signalling pathway that mediates
302 communication between pancreatic β cells and macrophages, impairing islet homeostasis.
303
304 **Molecular mechanism underlying the engagement of insB:9-23 with Olfr109**
305 The different activities of the various secreted insulin peptides towards Olfr109
306 suggested that recognition of the primary peptide sequence by Olfr109 is an important
307 determinant for ligand-Olfr109 engagement (Fig. 3I-3J and Table S2). To characterize the
308 engagement of insB:9-23 within Olfr109, we performed alanine (Ala) scanning mutagenesis
309 of Olfr109 to alter all residues in the extracellular loop (ECL) and the upper half of the
310 seven-transmembrane bundle (7TM), which have been suggested to form the ligand binding
311 pocket for most solved class A GPCR structures (Fig. 5A). 19 of the 163 examined mutant
312 receptors were not expressed on the surface, even after the amounts of transfected plasmids
313 were adjusted, and were excluded from further screening (Fig. S8). We first performed a
314 concentration-dependent arrestin recruitment assay for Olfr109 mutants as a convenient
315 approach to determine the functional EC50 and Emax values. The mutants with severe effects
316 on arrestin function were then subjected to a ligand binding assay to determine their affinity
317 for Olfr109 (Fig. 5A). In total, mutations in 18 residues in the TM bundles and 5 residues in
318 the ECLs significantly impaired arrestin recruitment by Olfr109 in response to insB:9-23
319 engagement (Fig. 5B, Fig. S9A and Table S4). Among these residues, 10 residues in TM1,
320 TM2, TM4 and TM5 and 2 residues in extracellular loop 2 (ECL2) impaired the binding of
321 insB:9-23 with Olfr109 (Fig. 5C and Table S5). Therefore, the ligand binding pocket of
322 Olfr109 interacting with peptide agonists is composed primarily of TM1-TM2, TM4-TM5
323 and ECL2.
324 To further define the hot spot interactions governing the recognition of insB:9-23 by
325 Olfr109, we carried out alanine scanning mutagenesis to characterize the effects on the
326 peptide agonist insB:9-23 and then paired the interactions of the mutants with the key Olfr109
327 residues by comparing the binding of individual peptide mutants with that of the wild-type
328 peptide for all receptor mutations with significant loss of binding ability (Fig. 5A, Auxiliary
329 Supplementary Table 3). For a receptor mutation that severely impaired the response to
330 wild-type insB:9-23 but had much less severe effects on the response to an insB:9-23 peptide
331 with a selective alanine substitution, the receptor mutation and insB:9-23 alanine substitution

could be paired with each other to identify potential hot spot interactions(*31*). Importantly, the N-terminal residues S9, H10 and L11, as well as V18 in the middle region of insB:9-23, were identified by both arrestin recruitment and ligand binding assays as key residues mediating Olfr109 interactions (Fig. 5D, Fig. S9B and Table S6). The importance of the N-terminal residues was further confirmed by the serial truncation data (Fig. S9C-S9D). Further scanning of pairing between insB:9-23 peptide mutants and the receptor mutants indicated that the specific interactions of $S9^{InsB}$ with $P77^{2.59}$, $H10^{InsB}$ with $F152^{4.55}$ and $Y153^{4.56}$, $L11^{InsB}$ with $M160^{4.63}$ and $T161^{4.64}$, and $V18^{InsB}$ with $F166^{ECL2}$ and $F167^{ECL2}$ are the potential hot spot interactions between Olfr109 and insB:9-23 (Fig. 5E, Table S7) (the superscripts indicate the Ballesteros-Weinstein numbers(*32*)). Importantly, whereas separate mutation of $H10^{InsB}$ /$L11^{InsB}$ /$V18^{InsB}$ to aspartic acid or mutation of their corresponding putative binding residues $F152^{4.55}$/$T161^{4.64}$/$F166^{ECL2}$ to arginine dramatically impaired the binding between the peptide and receptor, complementary mutations of the interacting pairs to build a favored charge interaction effectively restored the binding (Fig. S9E-S9G). Collectively, this mapping of mutational effects coupled with the results of the arrestin recruitment, ligand binding and pairing assays indicated that insB:9-23 binds to Olfr109 via insertion of its N-terminus into the 7TM bundle, with extra interactions provided by engagement of the middle part of the peptide with the ECL2 region of the receptor. Olfr109 specifically recognized insB:9-23 through selective hot spot interactions mediated by the hydrophobic residues contributed by TM2-TM4, as well as ECL2.

More than 170 missense SNPs have been reported in Human database (Fig.5F). Notably, at least five single nucleotide polymorphism (SNP) occurred at the identified potential ligand-binding sites of OR12D3, which is the homologues receptor of OLFR109 in human. Except for $Y71F^{2.53}$, mutants of $C167W^{ECL2}$, $Y71S^{2.53}$, $T31S^{1.41}$, and $T31N^{1.41}$ significantly impaired both arrestin recruitment and insB:9-23 binding to OR12D3 (Fig. 5G,Fig.S9H). These data not only supported the interacting mode between OLFR109/OR12D3 and insB:9-23, but also indicated potential clinical relevance of these naturally occurring OR12D3 mutations, which might be more resistant toward diabetes development.

Pharmacological blockade of Olfr109 by pepducin improved glucose metabolism in models of diabetes and obesity

Pepducins are short lipid-coupled peptides derived from the intracellular loops of their cognate receptors; they are effective allosteric regulators of GPCRs and are not only useful for studying the function of a particular GPCR but also have therapeutic potential(*33*). We designed a series of pepducins according to the Olfr109 sequence and evaluated their ability to modulate Olfr109 activity (Fig. 6A). Three pepducins—o109-i3, o109-i2-5 and o109-i2-6—exhibited dose-dependent inhibition of cAMP accumulation induced by forskolin

via Olfr109, with EC50 values of 811.5±121.3 nM, 574.3±74.5 nM and 236.8±26.2 nM, respectively (Fig. 6B and Fig. S10A-S10D). In particular, o109-i2-2 acted as an Olfr109 antagonist specifically for Gi activity in response to insB:9-23 stimulation, with an EC50 of 210.4±9.2 nM, but did not interact with other olfactory receptors or peptide hormone sensing GPCRs (Fig. 6C, Fig. S10E-10I). Moreover, the decreased insulin secretion and increased endoplasmic reticulum stress elicited by insB:9-23 treatment in pancreatic islets or MIN6 pancreatic β cells were significantly alleviated by o109-i2-2 administration, and these effects were dependent on Olfr109 expression (Fig. 6D-E).

Delighted by the effects of o109-i2-2 on improving islet functions, we then examined the effects of the pepducin Olfr109 antagonist in HFD-induced metabolic obesity and Akita diabetic mouse models. Treatment with o109-i2-2 significantly ameliorated the glucose metabolism disorder in both HFD-fed mice and Akita mice, and this effect was dependent on Olfr109 (Fig. 6F-6G, Fig. S10J-S10K). Therefore, we have developed a pepducin-based Olfr109-specific antagonist, and the effects of this pepducin suggested that pharmacological blockade of Olfr109 improved glucose homeostasis in mouse models of metabolic obesity and diabetes.

Conclusion

By screening all 278 mouse ORs with considerable homology to all ORs in *Homo sapiens*, we identified six ORs with relatively high expression levels in pancreatic islets that may actively participate in biochemical communications mediating islet functions. The expression of one of these six ORs, Olfr109, was found to be significantly increased in all models of obesity or diabetes. Specific expression of Olfr109 in pancreatic islets were supported by the RNAscope *in situ* hybridization, mRNA levels in GFP-labeled selective pancreatic cell types, radio-ligand binding and using *Olfr109*$^{-/-}$ mice. Interestingly, knockout of Olfr109 in vivo improved glucose homeostasis in both diabetes and obesity models, and overexpression of Olfr109 arrested insulin secretion from pancreatic β cells, suggesting that Olfr109 functions in islets as a potentiator of pathological conditions.

We then identified Olfr109 as a direct receptor for denatured insulin and several insulin peptides derived from “retired insulin”. A pathologically important previous finding is that not only functionally intact insulin in dense core granules but also old insulin granules containing retired insulin are secreted into the bloodstream in response to increased plasma glucose levels(*1-3*). Considerable amounts of insulin peptides derived from retired insulin are highly associated with diabetes, and recent studies have shown that these insulin peptides can be presented by MHC complexes to trigger immune responses(*25*). However, whether pancreatic β cells can sense the production of these peptides and other forms of misfolded

insulin remains unknown. Here, we not only presented solid evidence of an interaction between insB:9-23 and Olfr109 using radioligand binding methods and Olfr109 knockout models but also offered a detailed description of the interaction mode between insB:9-23 and Olfr109, thus providing mechanistic insight into the recognition of a peptide ligand by an OR at the molecular level. This knowledge could broadly impact the understanding of ligand recognition by this large family of receptors. Moreover, in response to engagement of insB:9-23 or denatured insulin, Olfr109 coupled to both Gi and β-arrestin-1, decreased the intracellular cAMP concentration to inhibit insulin secretion and promoted CCL2 production in β cells to mediate crosstalk with macrophages, finally facilitating the proliferation of islet-resident macrophages. Recent studies have demonstrated that local proliferation of islet-resident macrophages is significantly enhanced and plays key roles in islet inflammation and diabetes development; however, the underlying mechanism and exact regulation pathway are undefined(*16*, *34-36*). Here, our study presented a new scenario in which a particular signalling pathway governed by ORs in response to endogenous islet peptides modulated crosstalk between pancreatic β cells and macrophages, thus controlling the inflammatory process in pancreatic islets. Thus, Olfr109 may emerge as a pivotal autonomous control point for islet homeostasis via examination of the quality and quantity of peptide products secreted by β cells in an autocrine manner.

The dispensable role of Olfr109 in wild-type mice but negative effects under pathogenic conditions indicated that aberrant amplification of Olfr109 function may adeptly mediate disease-related conditions. By contrast, we have identified that several SNPs in the putative InsB 9:23 binding site of Olfr109 significantly decreased the signaling response downstream of Olfr109. Their clinical relevance awaits further investigation. Moreover, we developed a pepducin-based selective antagonist of Olfr109 that significantly improved glucose homeostasis in both the HFD-induced obesity and diabetic *Akita* mouse models. These findings indicate the new therapeutic potential of antagonizing the pancreatic islet-resident OR Olfr109. Collectively, the results of the present study expand our understanding of insulin biology by demonstrating that an insulin peptide can engage with an autonomous receptor and regulate local inflammation processes that intervene with islet homeostasis. Antagonizing Olfr109 could be a new therapeutic strategy for suppressing islet inflammation to treat obesity and diabetes.

Figure legends

Figure 1. Expression of olfactory receptors in mouse islets and the effects of Olfr109 deficiency on glucose homeostasis in diabetic *Akita* mice

(A) Phylogenetic tree showing the evolutionary relationship of mouse olfactory receptors (ORs) identified to have relatively high expression levels in pancreatic islets. The ORs expressed in islets are highlighted in red.

(B) qRT-PCR analysis of mRNA expression levels of six OR genes in pancreatic islets of wild-type (WT) male mice normalized to their corresponding levels in nasal olfactory epithelium.

(C) mRNA levels of six mouse OR gene homologues in human islets after stimulation with low concentration of glucose or high concentration of glucose. Data are from three independent experiments (n=3).

(D) mRNA levels of six OR genes in islets isolated from 8-week-old WT or Akita mice.

(E) mRNA levels of six OR genes in islets isolated from mice fed a normal chow diet (NCD) or a high-fat diet (HFD). Data are from three independent experiments (n=3).

(F) Effects of OLFR109 or OLFR110 overexpression in MIN6 pancreatic β cells on insulin secretion Data are from three independent experiments.

(G) Representative images colorimetric RNAscope in situ hybridization for Olfr109 (red) in pancreatic sections of WT and *Olfr109*$^{-/-}$ mice.

(H) Body weight changes in ins2$^{WT/WT}$*Olfr109*$^{+/+}$, ins2$^{WT/Akita}$*Olfr109*$^{+/+}$, ins2$^{WT/WT}$*Olfr109*$^{-/-}$, and ins2$^{WT/Akita}$*Olfr109*$^{-/-}$ mice.

(I-J) Energy expenditure (H) and respiratory quotient (I) values in ins2$^{WT/WT}$*Olfr109*$^{+/+}$, ins2$^{WT/Akita}$*Olfr109*$^{+/+}$, ins2$^{WT/WT}$*Olfr109*$^{-/-}$, and ins2$^{WT/Akita}$*Olfr109*$^{-/-}$ mice, as measured by indirect calorimetry.

(K-L) Plasma glucose levels (J) and insulin levels (K) in ins2$^{WT/WT}$*Olfr109*$^{+/+}$, ins2$^{WT/Akita}$*Olfr109*$^{+/+}$, ins2$^{WT/WT}$*Olfr109*$^{-/-}$, and ins2$^{WT/Akita}$*Olfr109*$^{-/-}$ mice during the glucose tolerance test.

(M) Insulin contents of the islets isolated from ins2$^{WT/WT}$*Olfr109*$^{+/+}$, ins2$^{WT/Akita}$*Olfr109*$^{+/+}$, ins2$^{WT/WT}$*Olfr109*$^{-/-}$, and ins2$^{WT/Akita}$*Olfr109*$^{-/-}$ mice. Data are from three independent experiments (n=3).

(N) Immunostaining (left panel) and quantitative analysis (right panel) of CD11c^{+} macrophages (red) in pancreatic sections from ins2$^{WT/WT}$*Olfr109*$^{+/+}$, ins2$^{WT/Akita}$*Olfr109*$^{+/+}$, ins2$^{WT/WT}$*Olfr109*$^{-/-}$, and ins2$^{WT/Akita}$*Olfr109*$^{-/-}$ mice. Scale bar: 100 μm. n = 6 mice per group; 4-7 random areas were selected from each islet section, and 10 sections were randomly selected from each mouse.

The bars indicate the mean ± SEM values. All data were statistically analysed using one-way ANOVA with Dunnett's post hoc test.

Figure 2. *Olfr109* deficiency improves glucose homeostasis in HFD-fed mice

(A) Body weight changes in WT and *Olfr109*$^{-/-}$ mice fed an NCD or HFD.

(B-C) Energy expenditure (B) and respiratory quotient (C) values in WT and *Olfr109*$^{-/-}$ mice fed an NCD or HFD, as measured by indirect calorimetry.

(D-E) Plasma glucose levels in WT and *Olfr109*$^{-/-}$ mice fed an NCD or a HFD during the insulin tolerance test (D) and glucose tolerance test (E).

(F-G) Plasma glucose (F) and insulin levels (G) in WT and *Olfr109*$^{-/-}$ mice fed an NCD or a HFD after refeeding.

(H) Insulin secretion from islets isolated from WT and *Olfr109*$^{-/-}$ mice fed an NCD in response to stimulation with high concentration of glucose. Data are from three independent experiments (n=3).

(I-J) Immunostaining (I) and quantification (J) of CD11c^{+} macrophages (red) in pancreatic sections of WT and *Olfr109*$^{-/-}$ mice fed an NCD or a HFD. Representative images are shown. Scale bar: 100 μm. n = 6 mice per group; 3-5 random areas were selected from each islet section, and 6-8 sections were randomly selected from each mouse.

(A-J) *P < 0.05; **P < 0.01; ***P < 0.001; ns, no significant difference; *Olfr109*$^{-/-}$ mice compared with WT mice fed the same diet. The bars indicate the mean ± SEM values. All data were statistically analysed using one-way ANOVA with Dunnett's post hoc test.

Figure 3. Identification of endogenous agonists of OLFR109

(A) Heatmap visualization of representative genes derived from whole transcriptome RNA-seq analysis of MIN6 cells transfected with si*Olfr109* or control siCon.

(B) Gene set enrichment analysis was conducted based on KEGG pathway annotation of the Gs/Gi-cAMP signalling pathway.

(C-D) Dose-dependent inhibition of forskolin-induced cAMP accumulation (C) and β-arrestin-1 recruitment to OLFR109 (D) in OLFR109-overexpressing HEK293 cells in response to incubation with supernatant.

(E-F) Dose-dependent inhibition of forskolin-induced cAMP accumulation (E) and β-arrestin-1 recruitment to OLFR109 (F) in OLFR109-overexpressing HEK293 cells in response to incubation with secretory granule fractions .

(G-H) Dose-dependent inhibition of forskolin-induced cAMP accumulation (G) and β-arrestin-1 recruitment to OLFR109 (H) in OLFR109-overexpressing HEK293 cells in response to incubation with the 5k secretory granule fraction.

(I-J) Maximum efficacy of cAMP inhibition (I) or β-arrestin-1 recruitment (J) in OLFR109-overexpressing HEK293 cells in response to the 15 peptides.

(K) Mass spectrum of the insB:9-23 peptide identified in the 5k secretory granule fraction.

(L) Saturation binding of ^{125}I-insB:9-23 to pancreatic islet membrane extracts derived from *Olfr109*$^{-/-}$ or WT mice.

(M) A best-fit linear correlation of the mRNA levels of OLFR109 in different tissues measured by qPCR with their protein levels of membrane fractions calculated from radioligand binding of ^{125}I-insB:9-23.

(N) Competitive binding curve of insB:9-23 in *Olfr109*-transfected HEK293 cells.

Figure 4. InsB:9-23-regulated functions and signalling via OLFR109

(A) Effects of insB:9-23 treatment on insulin secretion in islets derived from WT or *Olfr109*$^{-/-}$ mice. Data are from three independent experiments (n=3).

(B) Effects of insB:9-23 treatment on the cAMP concentration in islets derived from WT or *Olfr109*$^{-/-}$ mice. (n=3). Data are from three independent experiments (n=3).

(C) Plasma glucose levels during the glucose tolerance test in WT and *Olfr109*$^{-/-}$ mice treated with vehicle control or insB:9-23 .

(D) Heatmap visualization of chemokine signalling-related genes derived from whole transcriptome RNA-seq analysis of islets isolated from WT mice.

(E) Relative mRNA levels of *Ccl2* and *Ccl25* in the islets isolated from WT or *Olfr109*$^{-/-}$ mice treated with vehicle or insB:9-23.

(F) Immunostaining for CD11c (red) in pancreatic sections of WT and *Olfr109*$^{-/-}$ mice treated with insB:9-23 or vehicle control.

(G) mRNA levels of *Mertk*, *CD64* and *Olfr109* in macrophages and nonmacrophage cells derived from mouse pancreatic islets normalized to the corresponding expression levels in isolated primary pancreatic β cells. Macrophages were derived from wide-type mice islets by biotinylated mAbs against F4/80 and magnetic nanobeads conjugated to Streptavidin. Primary β cells were derived from *Ins2*^{cre}*Rosa*$^{lsl\text{-}GFP}$ mice islets by fluorescence-activated cell sorting (FACS).

(H) mRNA levels of Ki67 in macrophages from mouse pancreatic islets cultured with the supernatants of islets isolated from HFD-fed WT or *Olfr109*$^{-/-}$ mice.

(I) Effects of stimulation with insB:9-23 on CCL2 levels in the supernatant of pancreatic islets isolated from WT or *Olfr109*$^{-/-}$ mice.

(J) Effects of treatment with the CCR2 antagonist INCB3344 on the proportion of pancreatic islet-resident macrophages in mice.

(K) Effects of treatment with the CCR2 antagonist INCB3344 on Ki67 mRNA levels of pancreatic islet-resident macrophages in mice.

Figure 5. Alanine scanning and molecular simulation revealing the interaction mode between insB:9-23 and OLFR109

(A) Schematic representation of the screening and modelling strategies used to characterize the interaction mode between insB:9-23 and OLFR109.

(B-C) Alanine scanning identified important residues in the OLFR109 receptor that recognize insB:9-23 through a β-arrestin1 recruitment assay (B) and a ligand binding assay (C).

(D) Alanine scanning identified important residues in insB:9-23 that bind to the OLFR109 receptor through the β-arrestin1 recruitment assay (D) and ligand binding assay (E).

(E) Pairing of insB:9-23 mutants with WT OLFR109 and OLFR109 mutants through alanine scanning and a ligand binding assay. The Ki value for the binding of each insB:9-23 mutant to OLFR109 mutants was normalized to the Ki value of the same insB:9-23 mutant binding to WT OLFR109. The receptor mutants that did not show significantly decreased Ki values compared to those of the WT receptor when binding to a specific insB:9-23 mutant are highlighted.

(F) SNPs occurred at the potential ligand-binding sites of OR12D3.

(G) Affinity of insB:9-23 peptide binding to wide-type or selective single nucleotide polymorphisms (SNPs) of OR12D3.

Figure 6. Development of a pepducin-based OLFR109 antagonist that improved glucose metabolism in both diabetic *Akita* mice and HFD-fed mice.

(A) Amino acid sequences of OLFR109 pepducins.

(B) Dose-dependent inhibition of forskolin-induced cAMP accumulation in *Olfr109*-transfected HEK293 cells.

(C) The Olfr109-ICL2-2 (o109-i2-2) pepducin induced dose-dependent inhibition of the decrease in cAMP accumulation.

(D) Effects of o109-i2-2 on insulin secretion from pancreatic islets in response to stimulation with a high glucose concentration alone or in combination with insB:9-23.

(E) Effects of o109-i2-2 on the mRNA levels of the endoplasmic reticulum stress factors *Prdx5*, *Ptgs1*, *Ptgs2*, and *Sxbp1* in MIN6 pancreatic β cells.

(F) Effects of o109-i2-2 on plasma glucose levels during the glucose tolerance test in WT or *Olfr109*$^{-/-}$ mice fed a HFD for 13 weeks.

(G) Effects of o109-i2-2 on plasma glucose levels during the glucose tolerance test in ins2$^{WT/Akita}$*Olfr109*$^{+/+}$ and ins2$^{WT/Akita}$*Olfr109*$^{-/-}$ mice.

The bars indicate the mean ± SD values. All data were statistically analyzed using one-way ANOVA with Dunnett's post hoc test.

References and Notes:

1. W. Ying, W. Fu, Y. S. Lee, J. M. Olefsky, The role of macrophages in obesity-associated islet inflammation and beta-cell abnormalities. *Nat Rev Endocrinol* **16**, 81-90 (2020).
2. X. Wan *et al.*, Pancreatic islets communicate with lymphoid tissues via exocytosis of insulin peptides. *Nature* **560**, 107-111 (2018).

3. J. Wei, J. W. Yewdell, Peptide secretion triggers diabetes. *Nature* **560**, 33-34 (2018).
4. G. Glusman, I. Yanai, I. Rubin, D. Lancet, The complete human olfactory subgenome. *Genome Res* **11**, 685-702 (2001).
5. J. M. Young, B. J. Trask, The sense of smell: genomics of vertebrate odorant receptors. *Hum Mol Genet* **11**, 1153-1160 (2002).
6. S. J. Lee, I. Depoortere, H. Hatt, Therapeutic potential of ectopic olfactory and taste receptors. *Nat Rev Drug Discov* **18**, 116-138 (2019).
7. M. Spehr *et al.*, Identification of a testicular odorant receptor mediating human sperm chemotaxis. *Science* **299**, 2054-2058 (2003).
8. C. Wu *et al.*, Olfactory receptor 544 reduces adiposity by steering fuel preference toward fats. *J Clin Invest* **127**, 4118-4123 (2017).
9. E. Li *et al.*, OLFR734 Mediates Glucose Metabolism as a Receptor of Asprosin. *Cell Metab* **30**, 319-328 e318 (2019).
10. M. J. Kracht *et al.*, Autoimmunity against a defective ribosomal insulin gene product in type 1 diabetes. *Nat Med* **23**, 501-507 (2017).
11. M. Y. Donath, C. A. Dinarello, T. Mandrup-Poulsen, Targeting innate immune mediators in type 1 and type 2 diabetes. *Nat Rev Immunol* **19**, 734-746 (2019).
12. J. F. Mohan *et al.*, Unique autoreactive T cells recognize insulin peptides generated within the islets of Langerhans in autoimmune diabetes. *Nat Immunol* **11**, 350-354 (2010).
13. B. D. Stadinski *et al.*, Diabetogenic T cells recognize insulin bound to IAg7 in an unexpected, weakly binding register. *Proc Natl Acad Sci U S A* **107**, 10978-10983 (2010).
14. H. Modi, J. D. Johnson, Folding mutations suppress early beta-cell proliferation. *Elife* **7**, (2018).
15. Y. Riahi *et al.*, Inhibition of mTORC1 by ER stress impairs neonatal beta-cell expansion and predisposes to diabetes in the Akita mouse. *Elife* **7**, (2018).
16. W. Ying *et al.*, Expansion of Islet-Resident Macrophages Leads to Inflammation Affecting beta Cell Proliferation and Function in Obesity. *Cell Metab* **29**, 457-474 e455 (2019).
17. D. T. Jones, R. R. Reed, Golf: an olfactory neuron specific-G protein involved in odorant signal transduction. *Science* **244**, 790-795 (1989).
18. J. M. Choi *et al.*, Development of the main olfactory system and main olfactory epithelium-dependent male mating behavior are altered in Go-deficient mice. *Proc Natl Acad Sci U S A* **113**, 10974-10979 (2016).
19. A. Nakashima *et al.*, Agonist-independent GPCR activity regulates anterior-posterior targeting of olfactory sensory neurons. *Cell* **154**, 1314-1325 (2013).
20. F. Yang *et al.*, Allosteric mechanisms underlie GPCR signaling to SH3-domain proteins through arrestin. *Nat Chem Biol* **14**, 876-886 (2018).
21. J. S. Smith, R. J. Lefkowitz, S. Rajagopal, Biased signalling: from simple switches to allosteric microprocessors. *Nat Rev Drug Discov* **17**, 243-260 (2018).
22. Y. Wang, H. G. Dohlman, Regulation of G protein and mitogen-activated protein kinase signaling by ubiquitination: insights from model organisms. *Circ Res* **99**, 1305-1314 (2006).
23. S. Tan *et al.*, Type 1 diabetes induction in humanized mice. *Proc Natl Acad Sci U S A* **114**, 10954-10959 (2017).
24. D. G. Alleva *et al.*, A disease-associated cellular immune response in type 1 diabetics to an immunodominant epitope of insulin. *J Clin Invest* **107**, 173-180 (2001).

25. X. Wan *et al.*, The MHC-II peptidome of pancreatic islets identifies key features of autoimmune peptides. *Nat Immunol* **21**, 455-463 (2020).
26. D. J. Drucker, Mechanisms of Action and Therapeutic Application of Glucagon-like Peptide-1. *Cell Metab* **27**, 740-756 (2018).
27. Y. Kawano *et al.*, Colonic Pro-inflammatory Macrophages Cause Insulin Resistance in an Intestinal Ccl2/Ccr2-Dependent Manner. *Cell Metab* **24**, 295-310 (2016).
28. N. Nakamoto *et al.*, CCR9+ macrophages are required for acute liver inflammation in mouse models of hepatitis. *Gastroenterology* **142**, 366-376 (2012).
29. M. Y. Donath, S. E. Shoelson, Type 2 diabetes as an inflammatory disease. *Nat Rev Immunol* **11**, 98-107 (2011).
30. K. Eguchi, R. Nagai, Islet inflammation in type 2 diabetes and physiology. *J Clin Invest* **127**, 14-23 (2017).
31. R. Li *et al.*, Molecular mechanism of ERK dephosphorylation by striatal-enriched protein tyrosine phosphatase. *J Neurochem* **128**, 315-329 (2014).
32. V. Isberg *et al.*, Generic GPCR residue numbers - aligning topology maps while minding the gaps. *Trends Pharmacol Sci* **36**, 22-31 (2015).
33. G. Schneditz *et al.*, GPR35 promotes glycolysis, proliferation, and oncogenic signaling by engaging with the sodium potassium pump. *Sci Signal* **12**, (2019).
34. J. A. Ehses *et al.*, Increased number of islet-associated macrophages in type 2 diabetes. *Diabetes* **56**, 2356-2370 (2007).
35. B. Calderon *et al.*, The pancreas anatomy conditions the origin and properties of resident macrophages. *J Exp Med* **212**, 1497-1512 (2015).
36. H. Sell, C. Habich, J. Eckel, Adaptive immunity in obesity and insulin resistance. *Nat Rev Endocrinol* **8**, 709-716 (2012).

Acknowledgement:

We acknowledge support from the National Key Basic Research Program of China Grant (2019YFA0904200 to J.-P.S., 2018YFC1003600 to X.Y. and J.-P.S.), the National Science Fund for Excellent Young Scholars Grant (81822008 to X.Y.), the National Science Fund for Distinguished Young Scholars Grant (81773704 to J.-P.S.), the National Natural Science Foundation of China Grant (31701230 to Z.Y., 31900936 to F.Y.) and Innovative Research Team in University Grant (IRT_17R68 to X.Y.).

Author Contributions:

X.Y. and J.-P.S. conceived and initiated the project. X.Y. and J.-P.S. supervised the overall project design and execution. J.C., Z.Y. and X.-Y. G. performed metabolic and histological studies of mice. J.C., Z.Y., X.-Y. G., R.M., J.-Y.L. Z.-M. T. isolated mice islets and performed *ex vivo* experiments. J.C., M.-X. G., and R.M. performed immunofluorescence studies. J.C., Z.Y. and X.-Y. G. performed macrophage isolation and chemokine studies. J.C. and X.-Y. G. isolated and lysed β cell granules for mass spectrometry. J.C. and Z.Y. performed radioligand binding assay. X.Y. and J.-P.S. designed the screening assays for dissecting the interaction mode between insB:9-23 and OLFR109. J.C., X.-Y. G., M.-X. G., and R.M. performed

673 ELISA assay and BRET assay of OLFR109 mutants. X.Y. and J.-P.S. designed pepducins of
674 OLFR109. J.C., Z.Y., X.-Y. G. and M.-X. G. performed pepducin-based cellular and mice
675 experiments. Y.-F. X. provided human islets. X.Y., J.-P.S., J.C., and Z.Y. participated in data
676 analysis and interpretation. F.Y. provided insightful ideas and contributed to structural
677 modelling. X.Y. and J.-P.S. wrote the manuscript. All of the authors have seen and commented
678 on the manuscript.
679

Figure 1

Figure 2

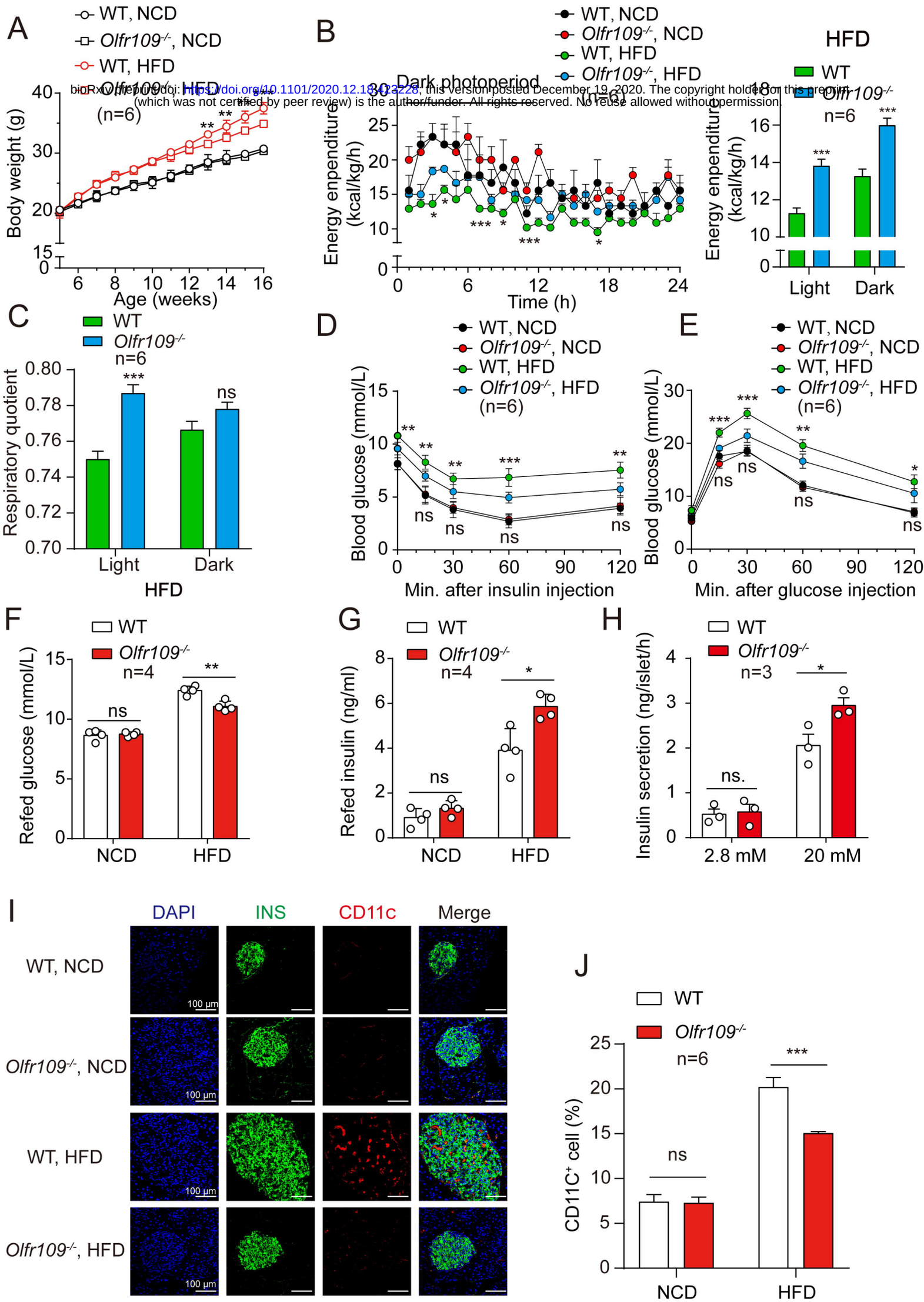

Figure 3

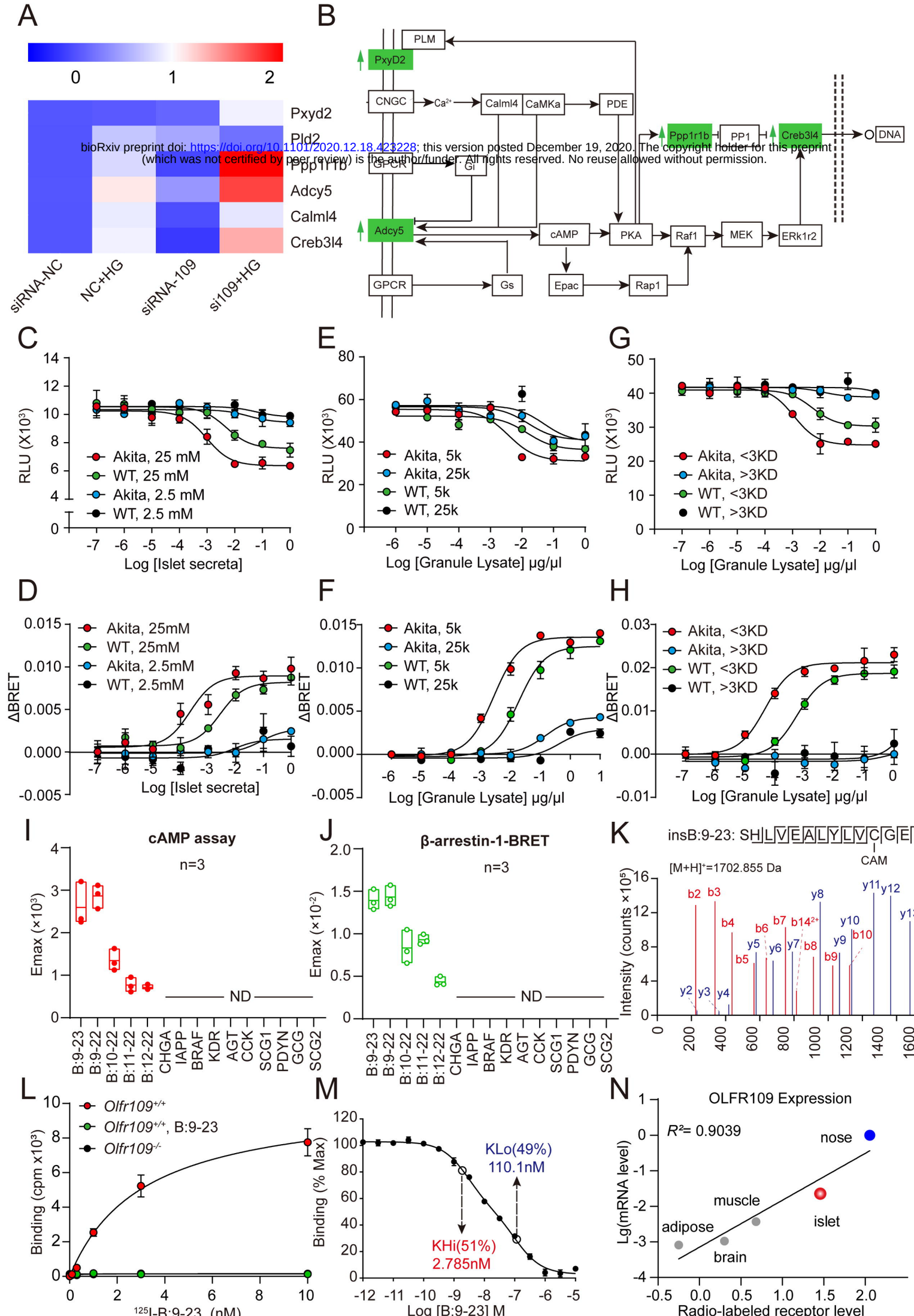

Figure 4

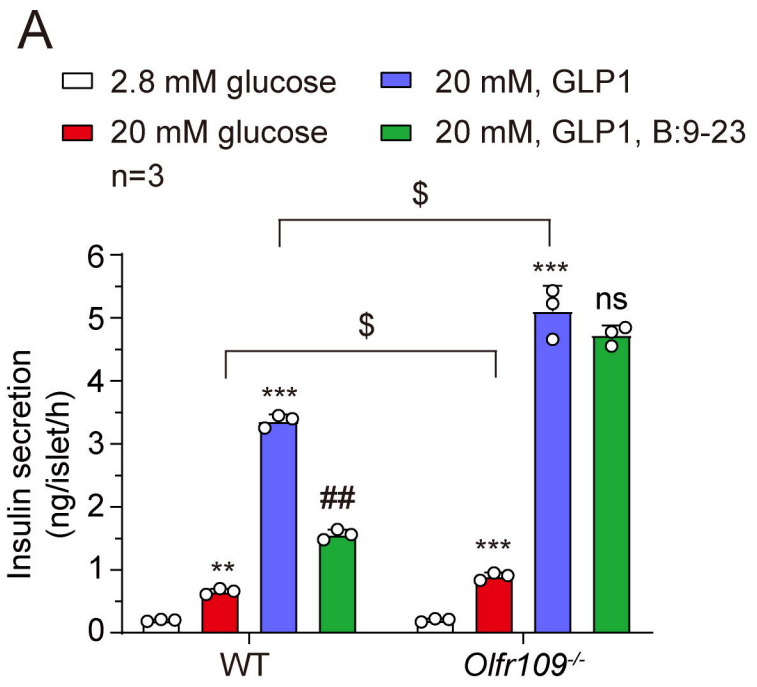
A
2.8 mM glucose
20 mM glucose
20 mM, GLP1
20 mM, GLP1, B:9-23
n=3
Insulin secretion (ng/islet/h)
WT
Olfr109-/-

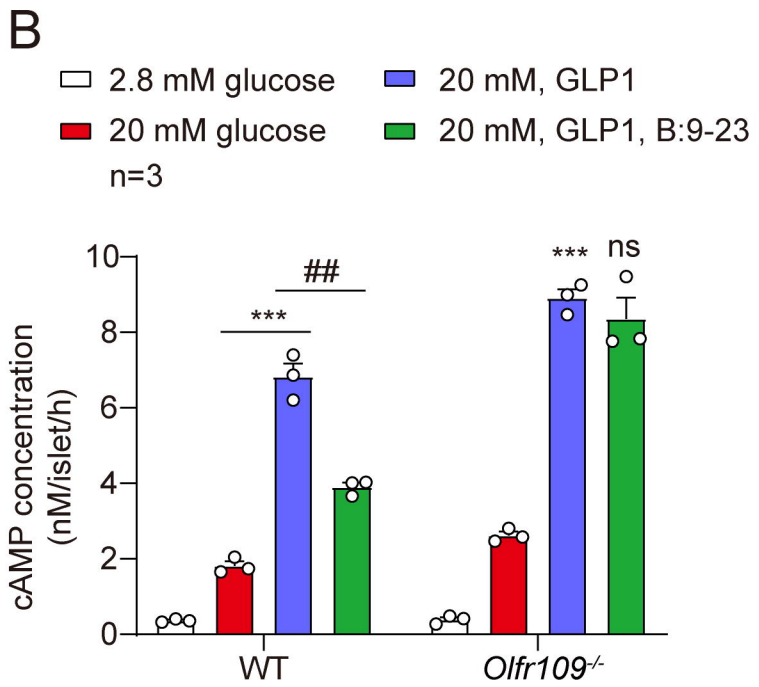
B
2.8 mM glucose
20 mM glucose
20 mM, GLP1
20 mM, GLP1, B:9-23
n=3
cAMP concentration (nM/islet/h)
WT
Olfr109-/-

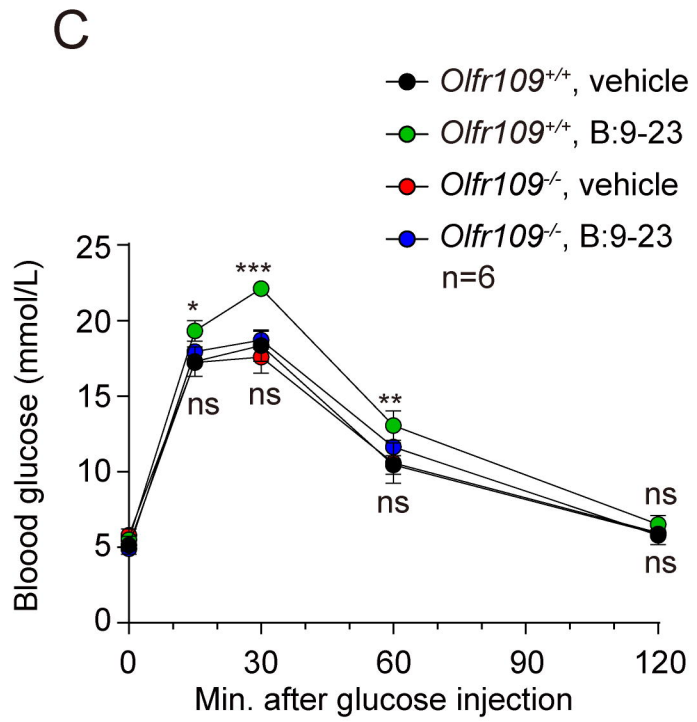
C
Olfr109+/+, vehicle
Olfr109+/+, B:9-23
Olfr109-/-, vehicle
Olfr109-/-, B:9-23
n=6
Blood glucose (mmol/L)
Min. after glucose injection

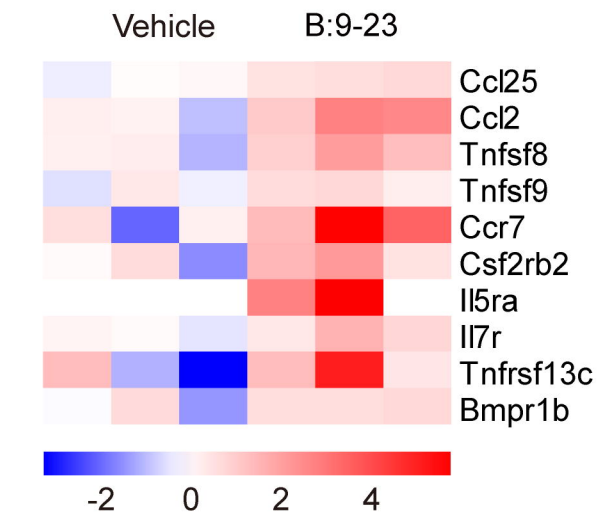
D
Vehicle
B:9-23
Ccl25
Ccl2
Tnfsf8
Tnfsf9
Ccr7
Csf2rb2
Il5ra
Il7r
Tnfrsf13c
Bmpr1b

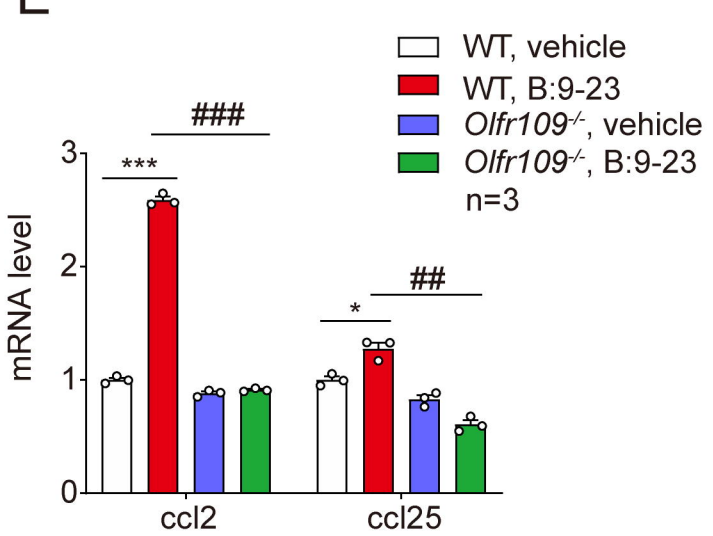
E
WT, vehicle
WT, B:9-23
Olfr109-/-, vehicle
Olfr109-/-, B:9-23
n=3
mRNA level
ccl2
ccl25

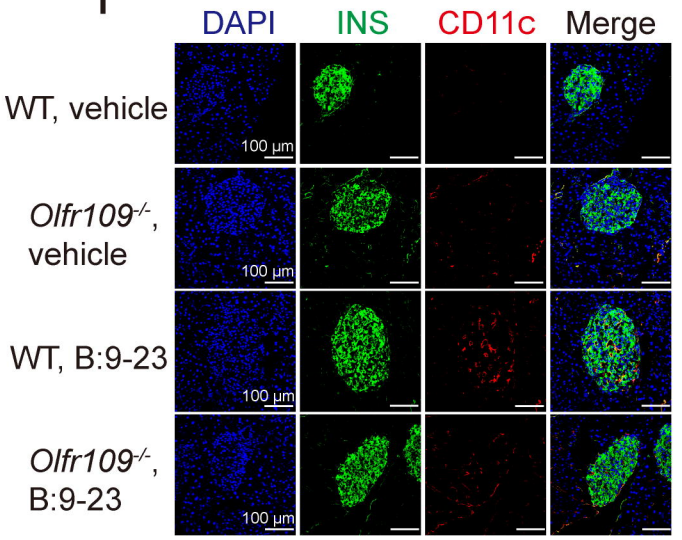
F
DAPI
INS
CD11c
Merge
WT, vehicle
Olfr109-/-, vehicle
WT, B:9-23
Olfr109-/-, B:9-23
100 μm

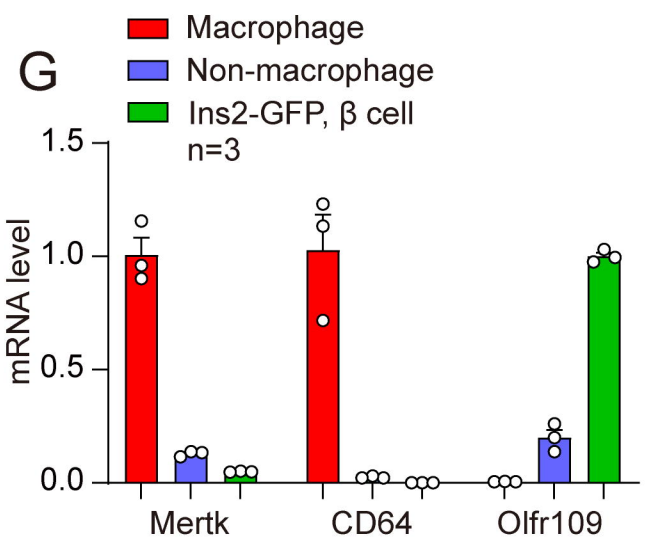
G
Macrophage
Non-macrophage
Ins2-GFP, β cell
n=3
mRNA level
Mertk
CD64
Olfr109

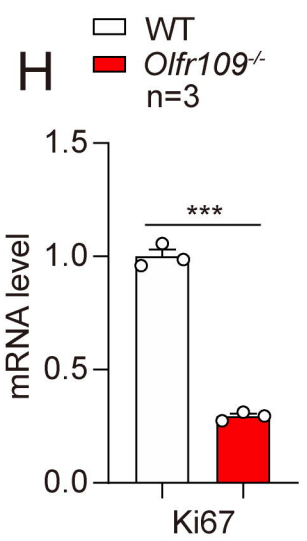
H
WT
Olfr109-/-
n=3
mRNA level
Ki67

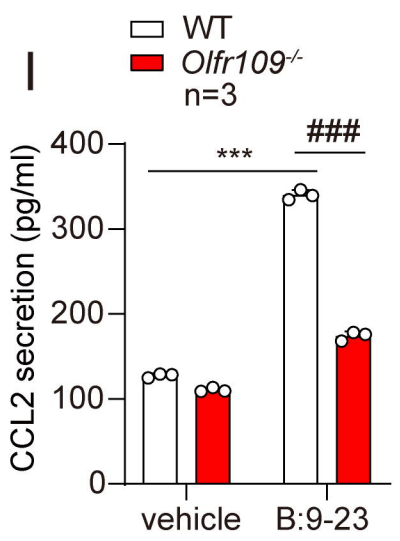
I
WT
Olfr109-/-
n=3
CCL2 secretion (pg/ml)
vehicle
B:9-23

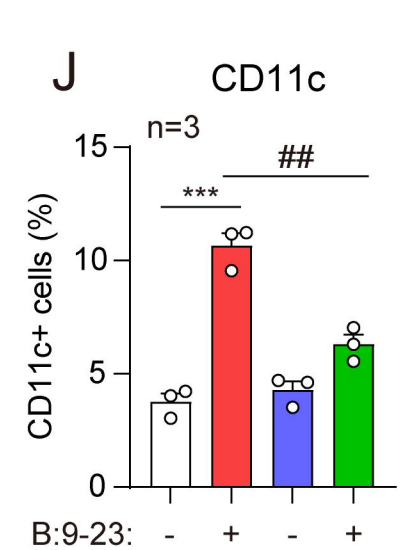
J
CD11c
n=3
CD11c+ cells (%)
B:9-23:
INCB3344:

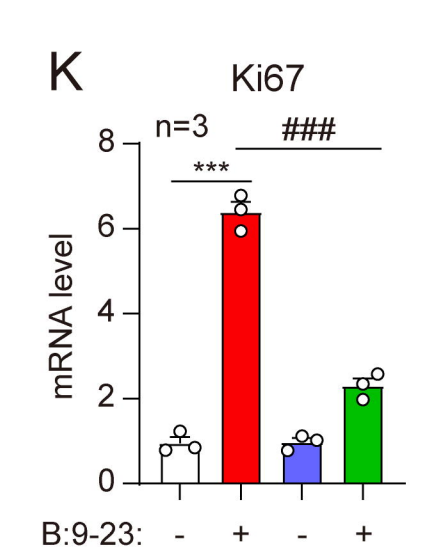
K
Ki67
n=3
mRNA level
B:9-23:
INCB3344:

Figure 5

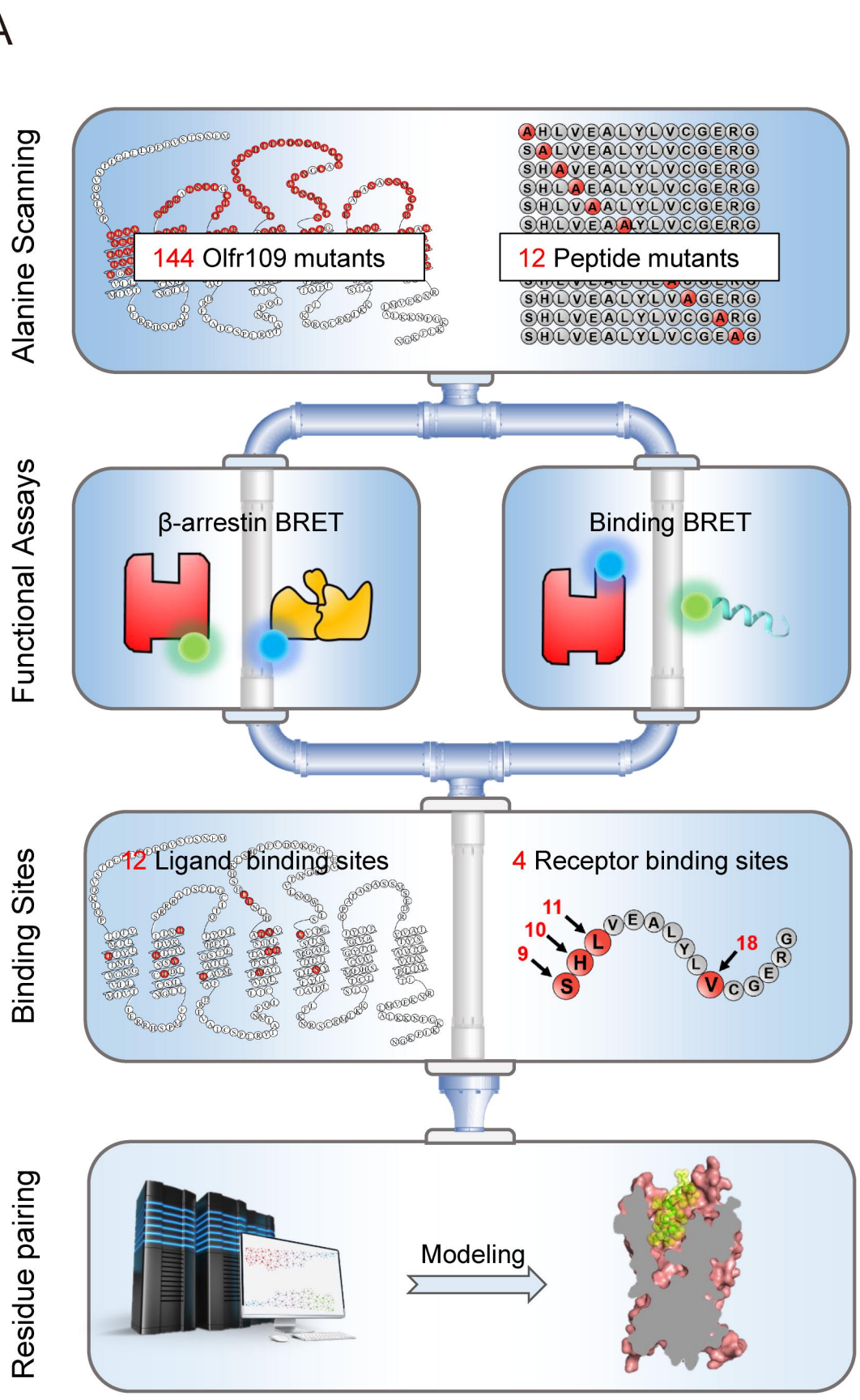

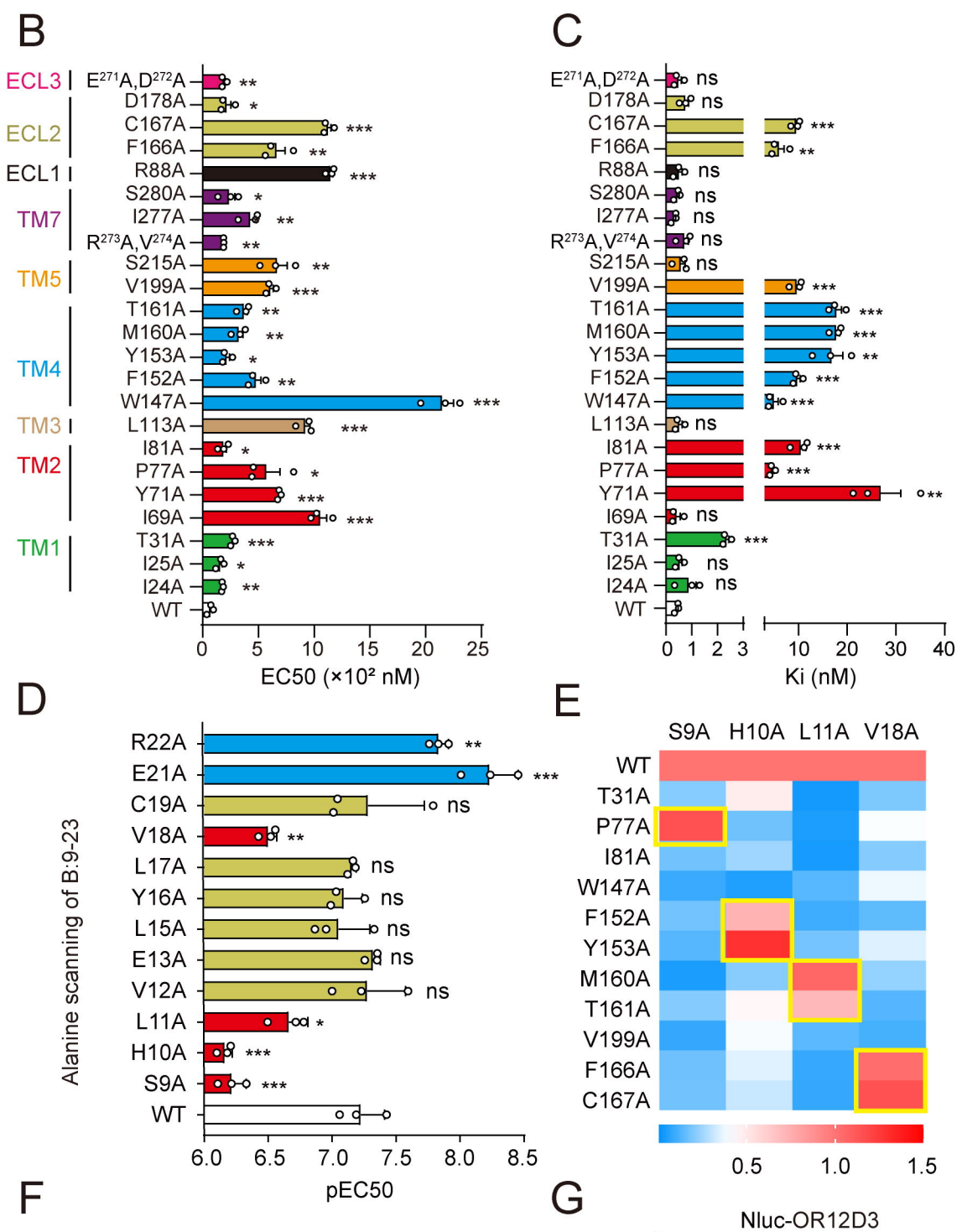

Change	SNP Number	Amino acid (Codon)
I31N	rs1355948032	I [ATC] → N [AAC]
I31S	rs1355948032	I [ATC] → S [AGC]
Y71F	rs567400895	Y [TAT] → S [TCT]
Y71S	rs567400895	Y [TAT] → F [TTT]
C167W	rs1400769112	C [TGT] → W [TGG]

Figure 6

A

Number	IC1-1	IC2-2	IC3-3
1	*N-pal*-LERRLHSPMYF-*NH2*	*N-pal*-DRFVAICSPLRYTAI-*NH2*	*N-pal*-LFKNRSCRMLKK-*NH2*
2		*N-pal*-RFVAICSPLRYTAIM-*NH2*	
3		*N-pal*-FVAICSPLRYTAIMN-*NH2*	
4		*N-pal*-VAICSPLRYTAIMNP-*NH2*	
5		*N-pal*-AICSPLRYTAIMNPQ-*NH2*	
6		*N-pal*-ICSPLRYTAIMNPQL-*NH2*